Check for updates

Reductive amidation of polylactic acid with nitro compounds using nickel based nanocatalysts†

Jie Gao, [ID] *[a] Lan Zhang,[b] Long Luo*[a,c] and Ning Wang [ID] *[b]

Here, we report carbon-supported Ni-nanoparticles as reusable catalysts for reductive amidation of nitro compounds with polylactic acid (PLA). These Ni-nanoparticle-based catalysts are prepared by synthesizing nickel-diamine ligands on a carbon support and subsequent pyrolysis under argon. Applying an optimal Ni-nanostructured catalyst, amidation of PLA with different nitro compounds in the presence of molecular hydrogen was performed to access amide products. Regarding improving the reaction efficiency, H_2O plays a positive role in the PLA hydrolysis process for lactic acid monomer production. Meanwhile, D_2O cannot promote PLA hydrolysis due to the lack of H atoms, which is vital for forming lactic acid monomers.

Green foundation

1. We present carbon supported nickel catalysts with isolated nanoparticles, which enable efficient reductive amidation of polylactic acid (PLA) plastics to afford amide products without producing any waste. These catalysts can be reused 5 times without significant activity loss. In addition, toluene and H_2O are the solvents used.

2. The global PLA market was valued at USD 1.5 billion in 2023 and is projected to reach USD 3.3 billion by 2028 (MarketsandMarkets™ website). The hot pursuit of PLA based products means that a serious issue of environmental and economic challenges caused by accumulating spent PLA is coming soon. This work presents a useful method to deal with PLA waste.

3. The coupling reaction of lactic acid and aniline can proceed automatically at higher temperatures. Chemists should develop more effective catalysts to enable this transformation under milder conditions.

Introduction

The development of plastic products from fossil fuels is one of the crowning achievements of the 20th century.[1–3] Fossil fuel-based plastics have become an essential part of manmade products, being applied in the diverse sectors of packaging, construction, agriculture, household goods, electronics, and automotive manufacturing.[1,4] In contrast, biomass-based polylactic acid (PLA) has attracted increasing interest as a sustainable plastic because it can be produced from starch, sugar, and cellulose. Noteworthily, the global PLA market was valued at USD

1.5 billion in 2023 and is projected to reach USD 3.3 billion by 2028 (MarketsandMarkets™ website). Government policies, growing awareness, and increasing demand from the Asia Pacific region are some of the factors driving the market for PLA (MarketsandMarkets™ website). The hot pursuit of PLA based products[5–8] means that a serious issue of environmental and economic challenges caused by accumulating spent PLA is coming soon. Though the spent PLA can be degraded into CO_2 and H_2O in a natural manner, the process is sluggish, and even worse, it is a CO_2-emitting and carbon resource waste process.[9] Therefore, strategies for upgrading PLA waste to value added chemicals are highly desired to achieve a circular plastic economy.

PLA has been used as a reactant for producing alanine chemicals through catalytic methods.[10–13] Amides are highly valuable compounds widely used in academic research and industries, and drug discovery.[14,15] Notably, amide functionality constitutes an integral part of a large number of pharmaceuticals and biomolecules, which play vital roles in the functions of these life science molecules. Considering the unique

[a]*Department of Chemistry, Wayne State University, 5101 Cass Avenue, Detroit, MI 48202, USA*

[b]*Faculty of Environment and Life, Beijing University of Technology, 100124 Beijing, China. E-mail: ning.wang.1@bjut.edu.cn*

[c]*Department of Chemistry, University of Utah, 315 S 1400 E, Salt Lake City, UT 84112, USA. E-mail: long.luo@utah.edu*

†Electronic supplementary information (ESI) available. See DOI: https://doi.org/10.1039/d4gc05635c

polyester structure of PLA, it may serve as a resource for *N*-substituted lactamide synthesis. From the viewpoint of sustainable development, a green and efficient approach is highly required.

Practical protocols with features of heterogeneous catalysts, milder conditions, and a hundreds of grams scale for *N*-substituted lactamide synthesis have not been reported. Only one example using homogeneous salts has been reported so far to synthesise *N*-substituted lactamide from anilines and PLA, accompanied by the production of waste (Fig. 1A).[16] The reduction of inexpensive and readily available nitroarenes is one of the most conventional methods by which amines are produced.[17–20] To the best of our knowledge no heterogeneous system can catalyse amidation of PLA by using amine or nitro compounds. In this regard, developing base metal catalysts, especially nanostructured materials, to perform the amidation of PLA in a more cost-effective and sustainable manner is highly desired and obviously attracts scientific interest. Due to their tuneable activities, selectivity, stability and recycling, supported nanoparticles are highly preferable.

Here, we report a practical protocol for the reductive amidation of nitro compound and PLA *via* a nickel-based heterogeneous catalyst using molecular hydrogen (Fig. 1B). Key to this transformation is the synergistic effect between metallic nickel and H_2O.

Results and discussion

Preparation of catalysts and catalytic activities

To prepare Ni-based nanoparticles, we first synthesized Ni–diamine complexes from $Ni(NO_3)_2 \cdot 6H_2O$ and 1,2-diaminobenzene. Specifically, the Ni-diamine complexes were formed *in situ* in methanol by simple stirring at room temperature. To the complexes in methanol, an active carbon support was added and further stirred for 12 h. Next, the corresponding Ni-diamine complexes were immobilized on active carbon to obtain catalyst precursors by removing methanol followed by drying. Finally, these immobilized materials were pyrolyzed at 400–1000 °C under argon to obtain supported Ni-nanoparticles (Fig. 2). Hereafter, these materials are denoted as Ni–L@Support-*T*. The L and *T* represent diamine ligand and pyrolysis temperature, respectively.

All the prepared Ni-materials were tested for amidation of PLA with 4-fluoronitrobenzene in the presence of molecular hydrogen. First, we tested Ni–L@C-*T* catalysts prepared at 400–1000 °C. On increasing the pyrolysis temperature, the activity of catalysts increased, and 800 °C was the best temperature to obtain the most active catalyst (Table 1, entries 1–3). On further increasing the pyrolysis temperature to 1000 °C, the activity of the corresponding material was slightly decreased (Table 1, entry 4), demonstrating that the pyrolysis temperature is of central importance. Interestingly, using toluene or H_2O solvent alone, the yield of desired products diminished (Table 1, entries 5 and 6). Next, Ni–L@Al_2O_3-800 catalysts were tested and the amide products were afforded with only 10% yield (Table 1, entry 7). The yield of amide products could be greatly improved up to 95% by increasing the reaction time to 24 hours (Table 1, entry 8). However, the Ni@C-800 material prepared without using ligand was active for the model reaction, but it gave worse conversion and product yield (Table 1, entry 9). The catalytic materials based on Fe, Co and Cu were tested and exhibited less activity compared to Ni–L@C-800 (Table 1, entries 10–12). The material L@C-800 was inactive for the model reaction, demonstrating that nickel is the active site for this reaction (Table 1, entry 13). As shown in Table S1,† nickel nanocatalysts are the active materials for reduction of nitro compounds. The mechanism of nitro reduction is shown in Fig. S1.† First, the nitro group was chemically adsorbed by nickel sites, and then it was gradually reduced to the amino group in the presence of molecular hydrogen.

Characterization of the Ni-based catalysts

As shown in Table 1, we have found that the catalytic performance is highly dependent on the pyrolysis temperatures. Thus, we conducted characterization studies using XRD, XPS, Raman spectroscopy, and TEM to understand the features of these samples (Ni–L@C-400, Ni–L@C-600, Ni–L@C-800, and Ni–L@C-1000).

As shown in Fig. 3a, metallic nickel with diffraction peaks at 44.5°, 52.0° and 76.4° were detected using XRD.[21–23] Interestingly, the intensity of these diffraction peaks increased with increasing the pyrolysis temperature from 400 to 1000 °C.
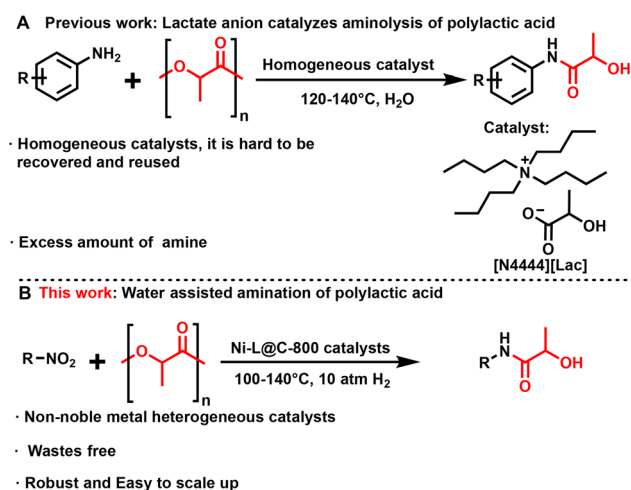

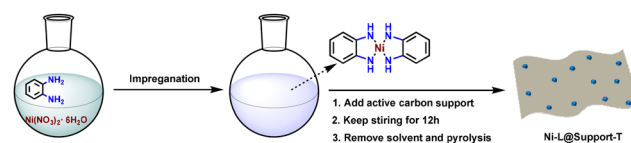**Fig. 1** Amidation of polylactic acid: the background and our work.

Fig. 2 Preparation of supported nickel nanoparticles by the immobilization and pyrolysis of the Ni–diamine complex on an active carbon support.

Table 1 Screening of catalysts for PLA amidation

Entry	Catalyst	T (°C)/t (h)	Solvent	Conversion of **1**, %	Yield, % 2	Yield, % 3
1	Ni–L@C-400	140/16	0.8 mL of toluene + 0.2 mL of H_2O	<1	<1	<1
2	Ni–L@C-600	140/16	0.8 mL of toluene + 0.2 mL of H_2O	40	24	15
3	Ni–L@C-800	140/16	0.8 mL of toluene + 0.2 mL of H_2O	69	30	37
4	Ni–L@C-1000	140/16	0.8 mL of toluene + 0.2 mL of H_2O	55	25	30
5	Ni–L@C-800	140/16	1 mL of toluene	60	58	<1
6	Ni–L@C-800	140/16	1 mL of H_2O	4	3	<1
7	Ni–L@Al$_2$O$_3$-800	140/16	0.8 mL of toluene + 0.2 mL of H_2O	26	16	10
8	Ni–L@C-800	140/24	0.8 mL of toluene + 0.2 mL of H_2O	>99	4	95
9	Ni@C-800	140/24	0.8 mL of toluene + 0.2 mL of H_2O	26	9	16
10	Co–L@C-800	140/24	0.8 mL of toluene + 0.2 mL of H_2O	26	9	16
11	Co–L@C-800	140/24	0.8 mL of toluene + 0.2 mL of H_2O	<1	<1	<1
12	Fe–L@C-800	140/24	0.8 mL of toluene + 0.2 mL of H_2O	<1	<1	<1
13	L@C-800	140/24	0.8 mL of toluene + 0.2 mL of H_2O	<1	<1	<1

Reaction conditions: 0.5 mmol of 4-fluoronitrobenzene, 30 mg of PLA, 20 mg of catalyst (3 mol% Ni), 20 bar H_2, solvent, 140 °C, 16–24 h, yields were determined by NMR using acetonitrile as the standard. The nickel content was determined to be 4.4 wt% by ICP-OES.

The binding energy of nickel shifted from 855.66 eV to 855.06 eV as the pyrolysis temperature increased from 400 to 1000 °C, indicating that the electron density of nickel increased gradually (Fig. 3b).[24,25] From the N 1S XPS, pyridinic N, pyrrolic N, graphitic N, and pyrrolic *N*-oxide species are observed at around 398 eV, 400 eV, 401 eV and 403 eV in these four samples (Fig. S2†).[26,27] However, the percentage ratio of these four types of nitrogen varies depending on the pyrolysis temperatures, and Ni–L@C-800 has the highest ratio of pyridinic N and pyrrolic N (Fig. S2†). Furthermore, we fitted the Ni $2P_{3/2}$ XPS spectra of these four samples to explore the surface nickel states (Fig. S3†). The samples of Ni–L@C-400 and Ni–L@C-600 exhibited only the peak of Ni_2O_3 located at around 855.5 eV. Meanwhile NiO located at around 854.5 eV was observed in Ni–L@C-800 and Ni–L@C-1000. In addition, $Ni(OH)_2$ and NiC were observed in Ni–L@C-1000. The TEM images of Ni–L@C-800 showed that nickel nanoparticles are distributed with an average particle size of 31.5 nm (Fig. 3e and f). However, the average particle size of Ni–L@C-600 was 27.5 nm (Fig. S4†), which is a little smaller than that of Ni–L@C-800. However, compared with Ni_2O_3, the reduction of NiO to generate metallic Ni was relatively easier. This indicated that more metallic nickel will be generated in Ni–L@C-800 compared with Ni–L@C-600, which serves as the active sites for reduction of nitro compounds. The average particle size of Ni–L@C-1000 was determined to be 36.1 nm (Fig. S5†). The general TEM images of these samples are shown in Fig. S6.† The HRTEM images show that the nickel nanoparticles in Ni–L@C-1000 are obviously coated by carbon layers due to the higher pyrolysis temperature (Fig. S7d†). Consequently, NiC was detected in Ni–L@C-1000 using the XPS technique (Fig. S3†). In contrast, the encapsulation of nickel nanoparticles by carbon layers in
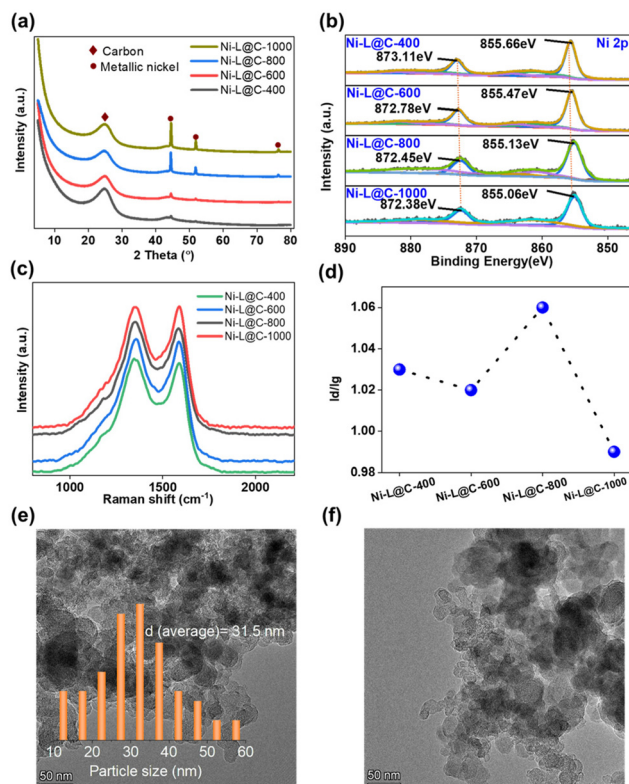

Fig. 3 Catalyst characterization. (a) XRD patterns and (b) Ni 2p XPS spectra of Ni–L@C-400, Ni–L@C-600, Ni–L@C-800, and Ni–L@C-1000. The surface Ni concentration of Ni–L@C-800 according to XPS is 1.21 at%. (c and d) The I_D/I_G ratios of Ni–L@C-400, Ni–L@C-600, Ni–L@C-800, and Ni–L@C-1000, obtained from Raman characterization. (e and f) TEM images of Ni–L@C-800.

Ni–L@C-400, Ni–L@C-600 and Ni–L@C-800 samples is not obvious due to the comparatively lower pyrolysis temperature. The thick carbon layers of Ni–L@C-1000 will cover the nickel sites and consequently prevent the interaction between reactant and nickel sites. As a result, Ni–L@C-1000 showed worse activity compared to Ni–L@C-800. Among all these four samples, Ni–L@C-800 has the most abundant surface NiO, which will be reduced to metallic nickel. This is the main factor that endows Ni–L@C-800 with the best catalytic activity. The structural defects of these four samples were analyzed using Raman spectroscopy. The D and G band peaks at around 1354 and 1599 cm^{-1} were observed in all these samples (Fig. 3c).[28] As shown in Fig. 3d, the I_D/I_G value of Ni–L@C-800 is the highest (I_D/I_G = 1.06), which indicates that it has the most abundant defect sites. As the pyrolysis temperature rises to 1000 °C, the value of I_D/I_G decreases from 1.06 to 0.99, indicating that a higher pyrolysis temperature increases the graphitization degree of the carbon support.[29,30]

Mechanism

H_2O is demonstrated to be of central importance in producing the amide products. Next, the reaction between 4-fluoroaniline and PLA was selected as the model reaction to explore the effect of H_2O. As shown in Fig. 4a, a higher reaction temperature was beneficial for increasing product yield. Then, on increasing the volume of H_2O from 0 to 0.2 mL, the product yield was increased significantly (Fig. 4b). Meanwhile, further increasing it from 0.2 to 2 mL, the product yield was decreased dramatically (Fig. 4b). In addition, 75% yield of amide products was detected in the H_2O system, while the reaction using D_2O solvent only produced 19% yield of amide products, probably due to the kinetic effect of the isotope (Fig. 4c). In the absence of any solvent, the product cannot be found by NMR spectra (Fig. 4c). Next, we carried out a group of control reactions (Fig. 5a) to research the effect of H_2O on PLA hydrolysis. Lactic acid (LA) was only detected with 44% yield in the presence of 0.2 mL of H_2O after 21 h of reaction, indicating additional H_2O is necessary for PLA hydrolysis in producing the LA monomer (Fig. 5a).[31] In contrast, the PLA hydrolysis process is much slower in the system involving D_2O as no lactic acid was detected under the same reaction conditions (Fig. 5a).

By exploring the effect of H_2O on the reaction between LA and 4-fluoroaniline, we found the yield of amide products gradually decreased on increasing the H_2O volume (Fig. 5b). Hence, we conclude that H_2O could promote the hydrolysis of PLA in the formation of a LA monomer, while an excess amount of H_2O is negative for producing amide products. So, a plausible mechanism was proposed, where nitro compounds were hydrogenated into aniline, while PLA went through hydrolysis and LA monomers were produced in the presence of H_2O. Finally, amide products were afforded through the reaction of aniline and LA just by heating at 140 °C (Fig. 5c).

After having designed the optimal catalyst and reaction conditions, we explored the applicability of the process for the amidation of different nitro compounds with PLA (Table 2).
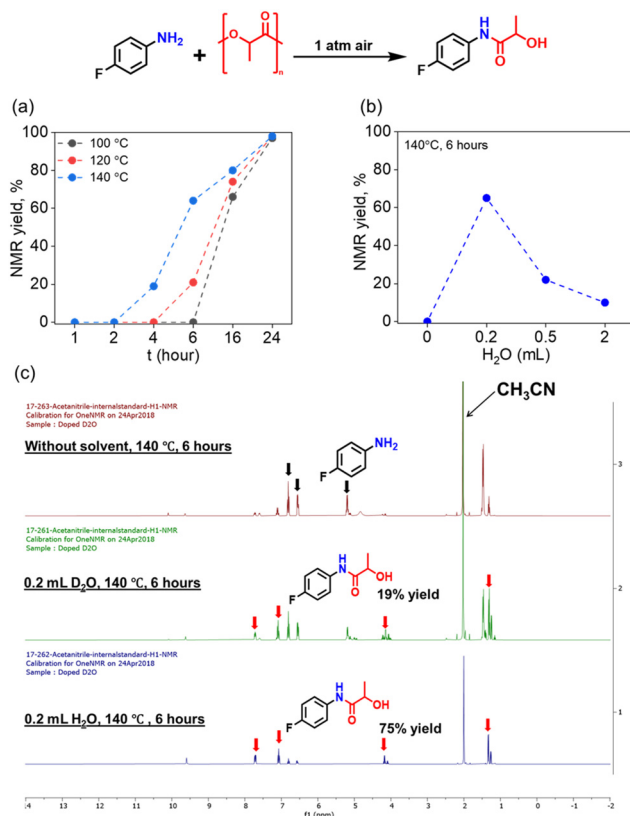

Fig. 4 The effect of (a) temperature and (b) H_2O volume on the product yield. (c) The corresponding NMR spectra. Reaction conditions: 2 mmol 4-fluoroaniline, 117 mg PLA, 100–140 °C, no catalysts, 0–2 mL H_2O or D_2O. Yields were determined by NMR using acetonitrile as standard.

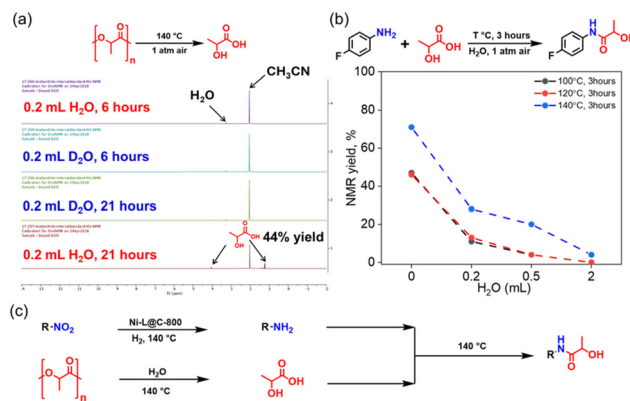**Fig. 5** The function of H_2O in PLA amidation. (a) Reaction conditions: 117 mg of PLA, solvent, no catalysts, 140 °C, 6–21 h. (b) Reaction conditions: 2 mmol of 4-fluoroaniline, 1.624 mmol of lactic acid, no catalysts. Yields were determined by NMR using acetonitrile as the standard. (c) Proposed mechanisms.

The aromatic nitro compounds bearing bromo, nitrile and sulfide functional groups could be well tolerated by this catalytic system (Table 2, entries 2–4). Similarly, the aliphatic nitro compound, (2-nitroethyl)benzene, was successfully converted

Table 2 Polylactic acid amidation in synthesis of *N*-substituted lactamide

Entry	Nitro compounds	H$_2$O/toluene, mL	*N*-substituted lactamide	Yield
1	nitrobenzene	0.2/0.8		80%
2	4-bromonitrobenzene	1/0.8		39%
3	4-nitrobenzonitrile	1/0.8		16%
4	methylthio-nitrobenzene	0.2/0.8		88%
5	phenethyl nitro	0.2/0.8		84%
6	3-nitropyridine	1/0.8		18%[a]

Reaction conditions: 0.5 mmol of nitrocompounds, 30 mg of PLA, 140 °C, 0.2 mL of H$_2$O, 20 mg of catalyst (3 mol% Ni), 20 bar H$_2$, solvent, 140 °C, 24 h. Yields were determined by NMR using acetonitrile as the standard. [a] Yields were determined by GC-MS.

into the corresponding amide with good yield (Table 2, entry 5). The yield of amide products synthesized from 3-nitropyridine was 18% (Table 2, entry 6).

To prove the synthetic utility and practicability of this protocol, the upscaling reaction was carried out on a 20 g scale (Fig. 6). A relatively lower yield compared to the 0.5 mmol scale was obtained. Finally, recycling and reusability of the Ni–L@C-800 catalyst were tested using the model reaction and it was found that this catalyst can be recycled and reused up to 5 times with a small loss of catalytic activity (Fig. 7). The recycled catalysts are subject to XRD, XPS and TEM characterization studies (Fig. S8 and S9†). The NiO species were detected using XRD and XPS. The average particle size was determined to be 48.85 nm using TEM, demonstrating that aggregation of metal particles occurred. The surface content of N is 4.35 at%. The loading amount of Ni–L@C-800 after each cycle is mentioned
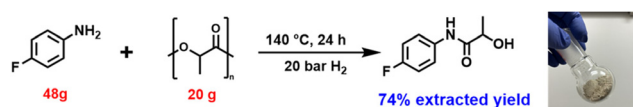
Fig. 6 The upscaling reaction. Reaction conditions: 48 g of 4-fluoronitrobenzene, 20 g of PLA, 13.3 g of catalyst, 20 bar H$_2$, solvent, 140 °C, 24 h.
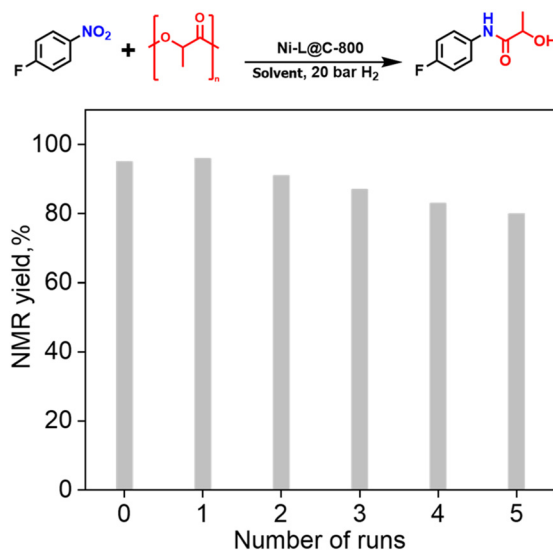
Fig. 7 Catalyst recycling for the reductive amidation of PLA with 4-fluoronitrobenzene. Reaction conditions: 0.5 mmol of 4-fluoronitrobenzene, 30 mg of polylactic acid, 20 mg of catalyst (3 mol% Ni), 20 bar H$_2$, 0.8 mL of toluene, 0.2 mL of H$_2$O, 140 °C, 24 h. Yields were determined by NMR using acetonitrile as the standard.

in Table S2.† No significant catalyst mass loss was observed. In addition, the loading amount of Ni is 3 mol%, which is the same as for the fresh material.

Conclusions

In conclusion, for the first time, we developed a non-noble metal based nanocatalyst for the reductive amidation of nitro compounds with polylactic acid plastic. Key to success for this reaction is the specific metallic nickel nanoparticles and defects of the catalysts. The H$_2$O is of central importance for amide product formation by promoting polylactic acid hydrolysis in producing lactic acid monomers. Using this Ni-based catalyst, both aromatic and aliphatic nitro compounds were transformed into their corresponding amide products. In addition to the synthetic performance, the recycling and reusability of Ni–L@C-800 were tested, too.

Author contributions

J. G. and L. L. planned the projects and wrote the manuscript. J. G. performed all the experiments. L. Z. and N. W. performed the characterization studies of catalysts and made manuscript corrections.

Data availability

The data supporting this article have been included as part of the ESI.†

Conflicts of interest

There are no conflicts to declare.

Acknowledgements

References

1 K. Hu, Y. Yang, Y. Wang, X. Duan and S. Wang, *Chem Catal.*, 2022, **2**, 724–761.

2 H. Li, H. A. Aguirre-Villegas, R. D. Allen, X. Bai, C. H. Benson, G. T. Beckham, S. L. Bradshaw, J. L. Brown, R. C. Brown, V. S. Cecon, J. B. Curley, G. W. Curtzwiler, S. Dong, S. Gaddameedi, J. E. García, I. Hermans, M. S. Kim, J. Ma, L. O. Mark, M. Mavrikakis, O. O. Olafasakin, T. A. Osswald, K. G. Papanikolaou, H. Radhakrishnan, M. A. Sanchez Castillo, K. L. Sánchez-Rivera, K. N. Tumu, R. C. Van Lehn, K. L. Vorst, M. M. Wright, J. Wu, V. M. Zavala, P. Zhou and G. W. Huber, *Green Chem.*, 2022, **24**, 8899–9002.

3 Y. Weng, C.-B. Hong, Y. Zhang and H. Liu, *Green Chem.*, 2024, **26**, 571–592.

4 R. Mi, L. Zeng, M. Wang, S. Tian, J. Yan, S. Yu, M. Wang and D. Ma, *Angew. Chem., Int. Ed.*, 2023, **62**, e202304219.

5 L. Jiang, X. Zhu, J. Li, J. Shao, Y. Zhang, J. Zhu, S. Li, L. Zheng, X.-P. Li, S. Zhang, H. Li, G.-J. Zhong and H. Xu, *Sep. Purif. Technol.*, 2024, **339**, 126708.

6 C. Wang, X. He, G. Zhu, X. Li, X. Zhu, R. Chen, S. Tian, X. Li, J. Zhu, J. Shao, J. Gao, G.-J. Zhong and H. Xu, *ACS Sustainable Chem. Eng.*, 2024, **12**, 9290–9300.

7 J. Yin, J. Zhang, Z.-Y. Chen, L.-F. Deng, D.-Z. Jia, H. Lin, J.-Z. Xu, H.-D. Huang, J. Lei, G.-J. Zhong and Z.-M. Li, *Macromolecules*, 2024, **57**, 10192–10207.

8 G. Zhu, C. Wang, T. Yang, N. Gao, Y. Zhang, J. Zhu, X. He, J. Shao, S. Li, M. Zhang, S. Zhang, J. Gao and H. Xu, *J. Hazard. Mater.*, 2024, **474**, 134781.

9 R. Cao, D. Xiao, M. Wang, Y. Gao and D. Ma, *Appl. Catal., B*, 2024, **341**, I23357.

10 S. Tian, Y. Jiao, Z. Gao, Y. Xu, L. Fu, H. Fu, W. Zhou, C. Hu, G. Liu, M. Wang and D. Ma, *J. Am. Chem. Soc.*, 2021, **143**, 16358–16363.

11 M. Cui, G. Liu, C. Ma, Z. Cao, Y. Ye, Y. Shen and X. Zhang, *New J. Chem.*, 2024, **48**, 6842–6847.

12 Y. Ma, X. Guo, M. Du, S. Kang, W. Dong, V. Nicolosi, Z. Cui, Y. Zhang and B. Qiu, *Green Chem.*, 2024, **26**, 3995–4004.

13 C. X. Liu, K. Liu, Y. Xu, Z. Wang, Y. Weng, F. Liu and Y. Chen, *Angew. Chem., Int. Ed.*, 2024, **63**, e202401255.

14 S. Tang, Z. H. Xu, T. Liu, S. W. Wang, J. Yu, J. Liu, Y. Hong, S. L. Chen, J. He and J. H. Li, *Angew. Chem., Int. Ed.*, 2021, **60**, 21360–21367.

15 J. Gao, L. Feng, R. Ma, B.-J. Su, A. M. Alenad, Y. Liu, M. Beller and R. V. Jagadeesh, *Chem Catal.*, 2022, **2**, 178–194.

16 F. Wu, Y. Wang, Y. Zhao, M. Tang, W. Zeng, Y. Wang, X. Chang, J. Xiang, B. Han and Z. Liu, *Sci. Adv.*, 2023, **9**, eade7971.

17 J. Gao, R. Ma, F. Poovan, L. Zhang, H. Atia, N. V. Kalevaru, W. Sun, S. Wohlrab, D. A. Chusov, N. Wang, R. V. Jagadeesh and M. Beller, *Nat. Commun.*, 2023, **14**, 5013.

18 R. V. Jagadeesh, A. E. Surkus, H. Junge, M. M. Pohl, J. Radnik, J. Rabeah, H. Huan, V. Schunemann, A. Bruckner and M. Beller, *Science*, 2013, **342**, 1073–1076.

19 D. Sokolova, T. C. Lurshay, J. S. Rowbotham, G. Stonadge, H. A. Reeve, S. E. Cleary, T. Sudmeier and K. A. Vincent, *Nat. Commun.*, 2024, **15**, 7297.

20 H. Jin, P. Li, P. Cui, J. Shi, W. Zhou, X. Yu, W. Song and C. Cao, *Nat. Commun.*, 2022, **13**, 723.

21 J. Gao, R. Ma, L. Feng, Y. Liu, R. Jackstell, R. V. Jagadeesh and M. Beller, *Angew. Chem., Int. Ed.*, 2021, **60**, 18591–18598.

22 N. L. Visser, O. Daoura, P. N. Plessow, L. C. J. Smulders, J. W. de Rijk, J. A. Stewart, B. D. Vandegehuchte, F. Studt, J. E. S. van der Hoeven and P. E. de Jongh, *ChemCatChem*, 2022, **14**, e202200665.

23 Z. Zou, Y. Shen, X. Zhang, W. Li, C. Chen, D. Fan, H. Zhang, H. Zhao and G. Wang, *Adv. Sci.*, 2024, **11**, 2309303.

24 J. Gao, Q. Jiang, Y. Liu, W. Liu, W. Chu and D. S. Su, *Nanoscale*, 2018, **10**, 14207–14219.

25 J. Ni, W. Leng, J. Mao, J. Wang, J. Lin, D. Jiang and X. Li, *Appl. Catal., B*, 2019, **253**, 170–178.

26 X. Bai, P. Hu, A. Li, Y. Zhang, A. Li, G. Zhang, Y. Xue, T. Jiang, Z. Wang, H. Cui, J. Kang, H. Zhao, L. Gu, W. Zhou, L.-M. Liu, X. Qiu and L. Guo, *Nature*, 2024, **634**, 80–84.

27 Q. Mo, N. Chen, M. Deng, L. Yang and Q. Gao, *ACS Appl. Mater. Interfaces*, 2017, **9**, 37721–37730.

28 J. Zhu and S. Mu, *Adv. Funct. Mater.*, 2020, **30**, 2001097.

29 S. Li, Y. Liu, H. Gong, K.-H. Wu, H. Ba, C. Duong-Viet, C. Jiang, C. Pham-Huu and D. Su, *ACS Appl. Nano Mater.*, 2019, **2**, 3780–3792.

30 D. S. Su, S. Perathoner and G. Centi, *Chem. Rev.*, 2013, **113**, 5782–5816.

31 F. Codari, S. Lazzari, M. Soos, G. Storti, M. Morbidelli and D. Moscatelli, *Polym. Degrad. Stab.*, 2012, **97**, 2460–2466.